Photochemistry in real space: batho- and hypsochromism in the water dimer

Alberto Fernández-Alarcón[a,b], José Manuel Guevara-Vela[a], José Luis Casals-Sainz[b], Aurora Costales[b], Evelio Francisco[b], Ángel Martín Pendás[b,*], Tomás Rocha Rinza[a,*]

[a]*Institute of Chemistry, National Autonomous University of Mexico, 04510 Mexico City, Mexico.*
[b]*Department of Analytical and Physical Chemistry, University of Oviedo, E-33006, Oviedo, Spain.*

Abstract

The development of chemical intuition in photochemistry faces several difficulties which result from the inadequacy of the one-particle picture, the Born-Oppenheimer approximation, and other basic notions used to build models. We show herein how real space approaches can be efficiently used to get valuables insights in photochemistry via a simple example of red and blue shift effects: the double hypso- and bathochromic shift in the low-lying valence excited states of $(H_2O)_2$. We demonstrate that (i) the use of these techniques allows to maintain the perturbative language used in the theory of intermolecular interactions even in the strongly interacting short-range regime; (ii) that it is one and only one molecule that gets photoexcited in each of the addressed excited states and (iii) that the electrostatic interaction between the in-the-cluster molecular dipoles provides a fairly intuitive rationalization of the observed batho- and hypsochromism. The methods exploited and illustrated in this paper are able to maintain the individuality as well as the properties of the interacting entities in a molecular aggregate, and thereby they allow to keep and build chemical intuition in general states, at any geometry and using a broad variety of electronic structure methods.

Keywords:

Partition of the excitation energy, Interacting Quantum Atoms, Hypsochromic and bathocromic effects, Hydrogen bond, Water dimer

*To whom correspondence should be addressed: trocha@iquimica.unam.mx, ampendas@uniovi.es

Electronic Supplementary Information (ESI) available: Computational details. Optimised geometries and IQA results for all the points throughout the examined potential energy curves. Ditto for dipole moments and dipole-dipole interaction energies.

Introduction

The creation and control of excited electronic states (EES) in condensed phases has become a field of paramount importance in modern photophysics and photochemistry [1] with wide-range technological implications. For example, the design of high efficiency solar cells,[2,3] organic light-emitting diodes,[4,5] luminescent sensors [6,7] or organic solid-state lasers,[8] should be based on a proper understanding of the nature of the EES involved in these systems. A similar situation arises when we try to rationalise relevant photobiological processes, such as cellular responses triggered by the absorption of a chromophore within a protein.[9,10]

The rational construction of chemically-engineered photoactive media is often faced with the considerable sensitivity of photoexcitation energies and the subsequent responses of the electronically species to their surroundings.[11–13] For instance, the protein environment of retinal shifts its first absorption maximum [13–15] with respect to the value measured in gas phase. Likewise, methanolic solutions decelerate some photoisomerization processes by an order of magnitude.[16] This circumstance represents both a problem and an opportunity, because if one can manipulate such environmental energy shifts, ΔE, then whole new windows of innovation are opened to the experimenter, such as fine-tuning of molecular photoswitches [17–19] or the development of bioluminiscent compounds for bioimaging.[20–22] There are many cases of such solvatochromic effects driven by non-covalent interactions in molecular aggregates. We can mention, for instance, the influence of π stacking in aromatic excimers [23] and DNA,[24], the solute-solvent interplay which affects the photoabsorption of chromophores in solution [25] or the important interactions between amino acids and cofactors found in protein-embedded photoactive molecules.[26–28] In particular, hydrogen bonds (HB) can generate noticeable changes onto the photochemical properties of a molecule or molecular cluster. An HB can ease internal conversions,[29,30] facilitate photoinduced electron transfers,[31,32] strongly affect metal-to-ligand charge transfers,[33,34] produce intra- and intermolecular proton transfers [35] or even

shift the photoabsorption energy by as much as 0.9 eV.[36]

Given this background, we examine herein how hydrogen bonds cause solvatochromic shifts. More specifically, we consider low-lying EES of $(H_2O)_2$ to inquire about the effects of HBs in photoexcitation energies. The water dimer is a simple archetype for the examination of such effects.[37] Its two lowest valence excited states $1\,^1A''$ and $2\,^1A'$ in $\mathcal{C}_s$ symmetry are known to exhibit HB-induced red and blue shifts.[38,39] This effect is usually referred to as a double hypsochromic and bathochromic shift with respect to an isolated monomer.[37]

On the other hand, these and other phenomena involving EES have over the years been theoretically described with the aid of sophisticated artillery in the field of computational photochemistry.[40] The accurate description of EES is, however, far more complicated than it is for ground states (GS) and therefore much of the effort concerning the theoretical study of EES has been employed to improve the core methods. Thus, the interpretation toolkit needed to build chemical insight from electronic structure calculations lags considerably behind in EES as compared with the GS. Nevertheless, there have been efforts to ameliorate this situation. For example natural bonding analisys[41] and the local chemical potential[42] have been used to study phenomena in the excited state. More recently, new tools have emerged, like the density overlap region indicator,[43] to get chemical insights about electronic excitations, or other techniques such as the absolutely localised molecular orbitals energy decomposition analysis.[44,45] or the adaptive natural density partitioning method[46] have been adapted to its use in the excited state.

These conditions lead to a rather unusual state of affairs. The most accurate methods of quantum chemistry allows for a precise characterization of potential energy surfaces, including diabatic and adiabatic couplings as well as conical intersections. However, no clear chemical picture of these processes exists. Something similar occurs regarding the batho- and hypsochromic shifts which conduce to solvatochromism. The community lacks methods to understand how changes in chemical bonding driven by non-covalent interactions cause blue and red shifts. This type of knowledge is essential to move forward from calculation to prediction and finally to control the generation and evolution of EES. Hereof, explanations based on distinct features of molecular orbitals, extremely powerful in ground states, are considerably

less useful in EES, because electron correlation and multi-configurational character do often ruin the one-particle picture.

Orbital invariant analyses either in position or momentum space are useful to ameliorate this problem. These analyses rely on reduced density matrices (RDMs),[47] which are essentially quantum mechanical joint probability distributions for electronic n-tuples. All together, these approaches are known as *real space analyses*[48] or quantum chemical topology (QCT) when restricted to position (or real) space. The QCT toolbox is well-known in ground states, and it offers chemically meaningful information in terms of atoms, functional groups, chemical bonds, molecular structure and electron pairs. This information might be provided, for example, through the quantum theory of atoms in molecules (QTAIM)[48] or the topological examination of the electron localisation function[49] or other related descriptors. Other approaches within the realm of QCT are (i) energy decompositions, e.g., with the interacting quantum atoms (IQA) method;[50,51] along with the use of effective one-electron functions with domain-averaged Fermi holes[52,53] or natural adaptive orbitals,[54] among others. However, the application of QCT techniques in the excited state is more scarce. Still, the QTAIM has been used in the study of the density of EES,[55–58] while the IQA methodology has been employed in the investigation of the energetic changes of a molecule in electronic excited states.[59] Moreover, the topology of the source function[60], the stress tensor[61] or the reduced density gradient[62] have been used to study different phenomena in EES.

Thus, this manuscript not only considers how the HB in $(H_2O)_2$ cause the double batho- and hypsochromic shifts in this system but also shows how new chemical insights about EES can be obtained from QCT methodologies. Hereof, we have recently put forward a method to dissect excitation energies computed with the black-box equation-of-motion (EOM) coupled-cluster singles and doubles (CCSD) approximation into atomic and interatomic contributions using the IQA formalism[63]. This new approach, denoted as IQA/EOM-CCSD, is particularly suitable for the examination of EES of molecular clusters such as $(H_2O)_2$ because of the size-consistency of the EOM-CCSD excitation energies. The coupling of this electronic structure approximation with IQA provides a unique way to detect which atoms and interactions are activated or depleted by photoabsorption in molecules and molecular clusters.

Overall, we offer a chemically appealing rationalisation of the blue and red shifts of $(H_2O)_2$ due to HB formation while we also highlight how the IQA/EOM-CCSD and other QCT techniques may yield relevant perspectives in the study of EES. We think that the future of these methods in photochemistry is brilliant and we expect to show herein some of their potential.

Computational and Theoretical Methods

Real space methods comprise the link between a computed wavefunction to chemical interpretations by associating spatial regions to chemical objects. This connection is made in the QTAIM at the atomic level, and $\mathcal{R}^3$ is divided into disjoint atomic basins Ω defined by the topological analysis of the electron density $\rho(\boldsymbol{r})$.[48] Each basin can be understood as an open quantum subsystem for which a density operator can be defined. These subsystems are in a mixed instead of a pure state with a given probability to display a particular number of electrons even for a general pure state of the global molecular system.

Several fields which are invariant under orbital rotations are either (i) sampled at particularly relevant points in $\mathcal{R}^3$ (usually the critical points of $\rho(\boldsymbol{r})$ or other scalar function) or (ii) integrated over the QTAIM basins. The expectation values of Dirac observables $\langle O \rangle$ are thus decomposed into additive atomic or interatomic contributions for one-electron and two-electron operators respectively. We are especially interested in rigorously partitioning the observables of a molecular complex into contributions attributed to every monomer in the adduct. The QTAIM is particularly well-suited for that purpose, and it can be used to assess how a molecular property (e.g. the electric dipole) changes due to the interaction with another species, or to understand how intermolecular charge transfers take place as described below.

Regarding the last case, the integral of the electron density over basin A,

$$\langle N_A \rangle = \int_A \rho(\boldsymbol{r}) \mathrm{d}\boldsymbol{r}, \tag{1}$$

provides the atomic population of this basin, which is the statistical average of the number of electrons in that region, i.e.,

$$\langle N_A \rangle = \sum_n n p_A(n). \tag{2}$$

Here, $p_A(n)$ is the probability that basin A contains n electrons. This statistical view of open systems[64] is useful to understand how a subsystem can maintain its average electron count upon interaction while the corresponding fluctuation, $\sigma^2(N_A)$, becomes non-vanishing. In other words, the subsystem can be found with different number of electrons that provide the same value of $\langle N_A \rangle$ once the interaction with other species has occurred, i.e., the subsystem exchanges electrons with its interacting partners.

Let us imagine two moieties A and B with N_A and N_B electrons, respectively, that interact with each other. We can envision two limiting behaviours. First, an integer number of electrons, let us say ΔN_A, are simply transferred from B to A. In this case, only one probability in the RHS of equation (2),

$$p_A(N_A + \Delta N_A) = 1, \tag{3}$$

is non-zero and

$$\langle N_A \rangle = N_A + \Delta N_A \qquad \text{with} \qquad \sigma^2(N_A) = -\text{cov}(N_A, N_B) = 0. \tag{4}$$

Second, several electrons are symmetrically exchanged between the fragments, so that more than one value of the probabilities $p_A(n)$, are different from zero and there is no change in the average population, i.e., $\langle N_A \rangle = N_A$ and $\sigma^2(N_A) \neq 0$. These limiting cases are readily associated with purely ionic and purely covalent bondings in chemistry. Intermediate situations lead, of course, to polar covalent bonds. We emphasise here that the covariance of the atomic populations, $\text{cov}(N_A, N_B)$, provides a measure of the number of shared electrons and therefore of covalency. Indeed,

$$\text{DI}(A, B) = -2\text{cov}(N_A, N_B), \tag{5}$$

constitutes a real space descriptor of the covalent bond order[65] which provides values equal to 1, 2 and 3 for ideal models of single, double and triple bonds respectively. Notice that full

charge transfers (equation (4)) lead to zero covalent bond order.

The partition of the electronic energy is of utmost importance. The IQA [50,51] method of wavefunction analysis considers QTAIM atoms to decompose exactly all the physical components of the electronic energy into atomic and interatomic contributions,

$$E = \sum_A E^A_{\rm net} + \sum_{A>B} E^{AB}_{\rm int}. \tag{6}$$

The net energy of atom A, $E^A_{\rm net}$, gathers all the intra-atomic energy components, i.e., the kinetic energy as well as the intrabasin (i) electron-nucleus attraction and (ii) electron-electron repulsion. On the other hand, the interatomic energy $E^{AB}_{\rm int}$ comprises all the pairwise additive interaction energies between all particles in basin A with those in basin B.[50] Because the QTAIM atoms can be joined to form composite basins that describe functional groups or molecules in molecular aggregates, the IQA net and interaction energies can equally well refer to any fragment or pair of moieties within the system. The interaction energy between two atoms or group of atoms can be further split into a term depending only on the average number of particles within a basin (as measured locally via the electron density) and another considering electron correlation. These terms are respectively called the IQA classical and exchange-correlation components,[51] and they fulfil the relation

$$E^{AB}_{\rm int} = E^{AB}_{\rm class} + E^{AB}_{\rm xc}. \tag{7}$$

The first term in the RHS of equation (7) describes the classical Coulombic interaction among a set of classical charges, and thereby it indicates ionic behaviour. The second term is non-zero when electrons are dynamically exchanged, which is the distinctive feature of covalency.

The consideration of the simplest molecule, $H_2{}^+$, is useful to illustrate the meaning of the above-discussed indicators. The electron of the system has a probability equal to 1/2 of being found in each atom. Therefore and according to equation (2), the average electron count per atom is

$$\langle N_A \rangle = \langle N_B \rangle = \sum_{n=0}^{1} n p_B(n) = 1/2. \tag{8}$$

Thus, there should be a classical Coulombic repulsion between the two half electrons equal to $1/(4R)$ at large internuclear distances R. The electron-nucleus attractions (twice $-1/2R$) and the nuclear repulsion ($1/R$) cancel each other in this regime and hence,

$$E_{\text{class}}^{\text{HH}} = \frac{1}{4R} \qquad \text{when} \qquad R \to \infty. \tag{9}$$

The interaction energy must vanish, $E_{\text{int}}^{\text{HH}} = 0$, at long range and then equations (7) and (9) imply that

$$E_{\text{xc}}^{\text{HH}} = -\frac{1}{4R} \qquad \text{when} \qquad R \to \infty, \tag{10}$$

which is a term that originates from the fluctuation of atomic populations. Such fluctuation in the atomic number of electrons gives rise to covalency whose associated bond order is given by formula (5),

$$\text{DI}(\text{H},\text{H}) = -2\text{cov}(N_A, N_B) = -2\left(\langle N_A N_B\rangle - \langle N_A\rangle\langle N_B\rangle\right) = 1/2. \tag{11}$$

The term $\langle N_A N_B\rangle$ vanish in the former equation because there is only one electron in the system and expression (8) is utilised. The covalent energy becomes in this way $-\text{DI}/(2R)$ in consistency with equation (10). This contribution is the first order term in a Taylor series expansion of E_{xc}^{AB},[66] and provides a vivid link between electron sharing, bond orders, and covalent energies.

Results and discussion

Our basic premise in this work is that QCT may be an useful tool to uncover how intermolecular interactions affect excitation energies in molecular clusters. As a first step to understand the effects of the HB on the excitation energies of $(H_2O)_2$, we briefly review the QCT picture of the changes undergone by an isolated water molecule when it is promoted to its first valence EES. Figure 1 shows the atomic basins of the three atoms of H_2O in the S_0 and S_1 states. The basins are separated by zero-flux interatomic surfaces. There is clearly an important redistribution of $\rho(\boldsymbol{r})$ when H_2O is excited from S_0 to S_1. We note that the electron density

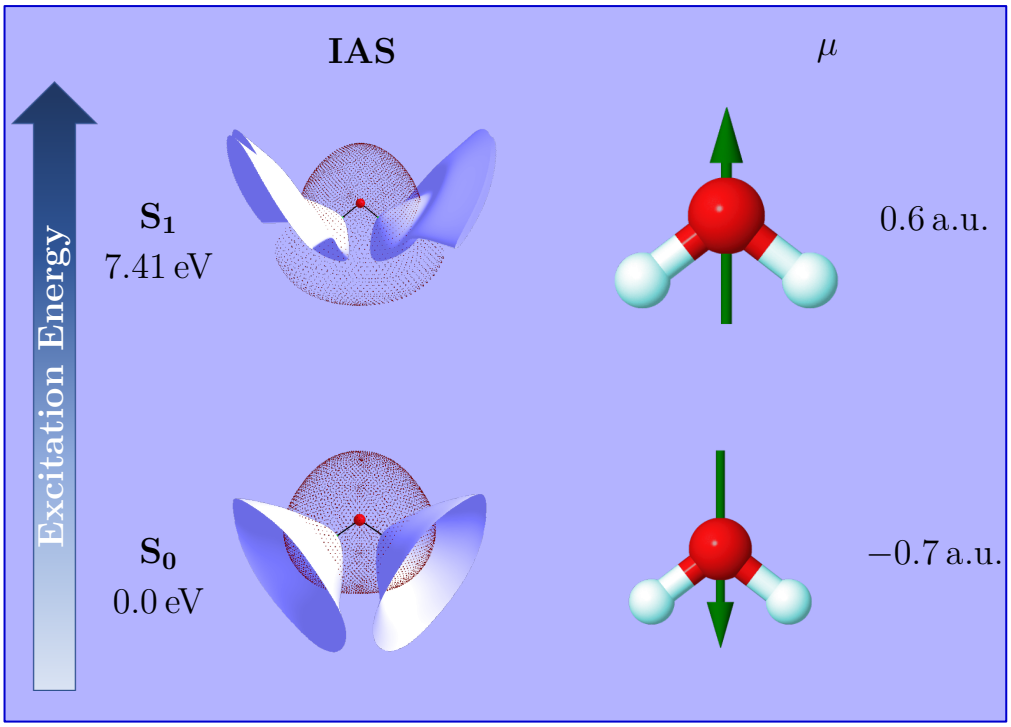

Figure 1: Excitation energy associated to the process $S_0 \rightarrow S_1$ in the water monomer (left), interatomic surfaces (center), and dipole moments (right) of the S_0 and S_1 states of the H_2O molecule.

which is mainly localised in the region corresponding to the lone pairs of the molecule in the GS, is displaced to the hydrogen basins away from the oxygen atom upon excitation. As shown in the right part of Figure 1, this electronic rearrangement leads to an inversion in the molecular dipole moment, a condition which will play a determining role in understanding the hypso- and bathochromic shifts of $(H_2O)_2$ addressed in this investigation.

The local energetic effects of the $S_0 \rightarrow S_1$ transition in the H_2O monomer are summarised in Table 1. We note that $|E_{\text{int}}^{\text{H}\cdots\text{H}}|$ becomes smaller as a consequence of this process. This reduction results from the covalent ($E_{\text{xc}}^{\text{O}-\text{H}}$) and the ionic ($E_{\text{class}}^{\text{O}-\text{H}}$) components of the O−H interaction. Both contributions decrease in magnitude in virtue of the $S_0 \rightarrow S_1$ excitation, althought the reduction in the absolute value of $E_{\text{class}}^{\text{O}-\text{H}}$ is substantially larger. The reduction in $|E_{\text{xc}}^{\text{O}-\text{H}}|$, the covalent contribution of the O−H bonding, contrasts with the increase in the delocalisation index of this interaction, $\Delta\text{DI}(\text{O},\text{H}) = 0.033$, as seen in the first row of Table 1. Despite the close connection between DI(A,B) and E_{xc}^{AB}, the greater DI in the excited state does not indicate a rise in covalency, but points instead to a increase of the zwitterionic

Table 1: QTAIM descriptors and components of the IQA partition energy for the singlet ground (S_0) and the first excited (S_1) states of the water molecule. Atomic units are used for the QTAIM indicators and eV for the IQA analyses.

	S_0	S_1
DI(O,H)	0.601	0.634
DI(H,H)	0.021	0.146
q^{O}	−1.166	−0.884
q^{H}	0.583	0.441
IQA energy decomposition		
E^{O}_{net}	−2035.29	−2034.10
E^{H}_{net}	−8.05	−7.70
E^{O-H}_{int}	−13.92	−10.91
E^{O-H}_{class}	−8.68	−6.44
E^{O-H}_{xc}	−5.24	−4.47
$E^{H\cdots H}_{int}$	3.71	3.18
$E^{H\cdots H}_{class}$	3.78	3.49
$E^{H\cdots H}_{xc}$	−0.07	−0.31

character of the interaction.[63,67] The decrease of $|E^{O-H}_{class}|$ is easier to explain: the transfer of electron density from the oxygen to the hydrogen atoms reduces the values of $|q^{O}|$ and $|q^{H}|$, which results in a reduction of $|E^{O-H}_{class}|$, the classical (ionic-like) contribution of the O−H bond energy. These energetic footprints accompany the dipole inversion of the $S_0 \rightarrow S_1$ excitation of the H_2O molecule (Figure 1).

We briefly mention that the interaction between the hydrogen atoms in the water monomer also reflects the changes in its electronic structure after photoexcitation, although the alterations in the H···H interaction are considerably less pronounced than those suffered by the O−H bond. There is a diminished repulsion between the hydrogen atoms due to the increase of electron density in their basins and the correspondingly smaller q^{H} values in the S_1 EES with respect to S_0. This change in the repulsion of H atoms within the H_2O molecule is reflected in the decrease of $E^{H\cdots H}_{class}$ following the $S_0 \rightarrow S_1$ excitation of the water monomer (Table

1). Likewise, the exchange-correlation component of the H···H interaction, $E_{\mathrm{xc}}^{\mathrm{H\cdots H}}$, becomes marginally more stabilising in the excited state.

To summarise, out of the $\approx 7.41\,\mathrm{eV}$ computed excitation energy, $2.89\,\mathrm{eV}$ are associated to intra-atomic phenomena ($1.60\,\mathrm{eV}$ come basically from the change in the charge of the oxygen atom) and the rest are related to the weakening of the O−H bonds. The photoexcited H_2O molecule is less strongly bound than its in its GS, a statement which matches the molecular orbital description of electronic excitations.

Photoexcitation energy shifts in $(H_2O)_2$

Now that we have some real space understanding of the changes occurring to the water molecule upon excitation, we focus our attention on the addressed $2\,^1A'$ and $1\,^1A''$ EES of $(H_2O)_2$. Figure 2 shows the excitation energies of this cluster as a function of the O···O distance for these two EES. Because of the size-consistency of the EOM-CCSD method, the excitation energy of the two states equals that of the water monomer at long O···O distances as expected. However, as the two H_2O units get closer and interact by means of an HB to form the dimer, a splitting of the two degenerate states takes place leading to the commonly referred double red and blue shifts of the water dimer. The $2\,^1A'$ and $1\,^1A''$ EES are respectively blue- and red-shifted with respect to the $S_0 \rightarrow S_1$ excitation of the H_2O monomer.

Because one can rigorously isolate the two interacting water molecules in $(H_2O)_2$ within the theoretical framework of QTAIM, we are offered the possibility to examine the effects of photoexcitation locally. In other words, we can determine how the HB donor and acceptor molecules within $(H_2O)_2$ are affected in each EES by virtue of photoexcitation. We first analyse descriptors related to the electron distribution to consider the different components of the excitation energy afterwards.

Table 2 gathers the values of the atomic charges in the ground and the first vertical two singlet EES of $(H_2O)_2$ at the S_0 equilibrium geometry. We find an electron transfer of $0.018\,e$ from the HB acceptor to the HB donor in the GS of the water dimer (left of Figure 3) as a natural consequence of this interaction in the system. There is a similar circumstance for the $2\,^1A'$ EES: $0.021\,e$ are removed from the HB acceptor to the HB donor as shown in the middle of Figure 3. Nevertheless, the situation changes for the $1\,^1A''$ EES, in which the electron flow

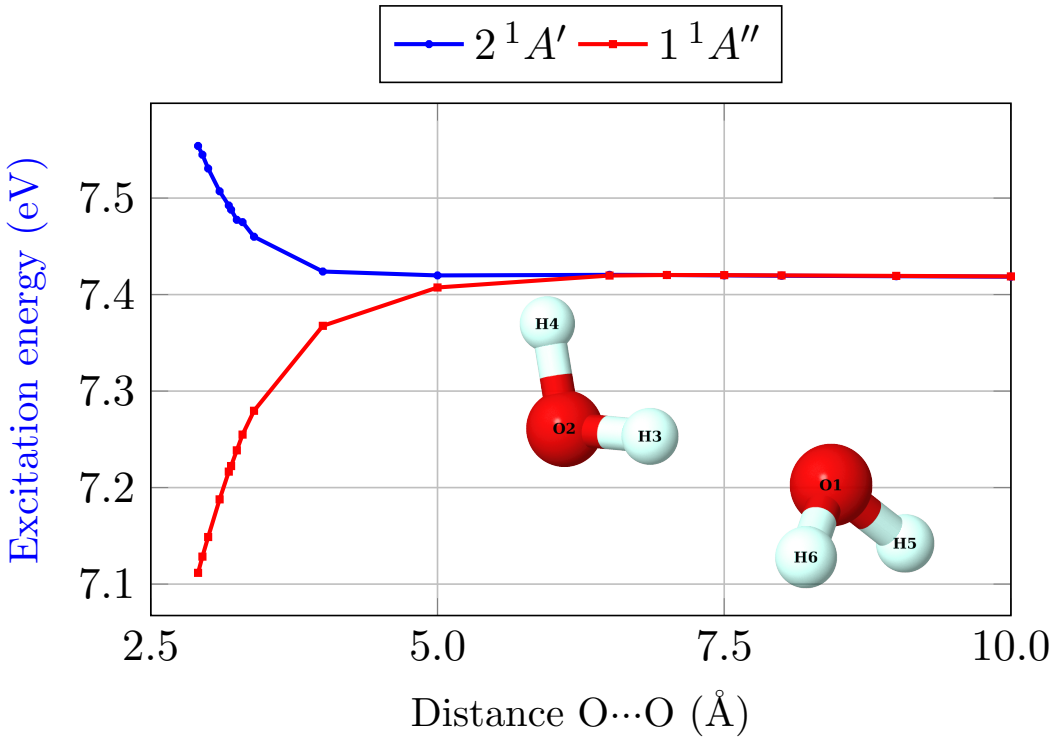

Figure 2: Excitation energy curves of the $2\,^1A'$ and $1\,^1A''$ states of $(H_2O)_2$ in the $\mathcal{C}_s$ configuration as a function of the O···O distance. The figure also shows the atomic labels used for further discussion in the paper.

is reversed. The right of Figure 3 displays an electron transfer of $0.09\,e$ from the HB donor to the HB acceptor in the $1\,^1A''$ state of $(H_2O)_2$. The charge transfer in the last-mentioned state of the water dimer is thus considerably affected.

The atomic charges of both H_2O units in the S_0 water dimer are similar to those found in the isolated GS monomer. Thorough rationalizations about the significance of QTAIM charges in HB formation have been previously reported and will not be reviewed here.[68] We

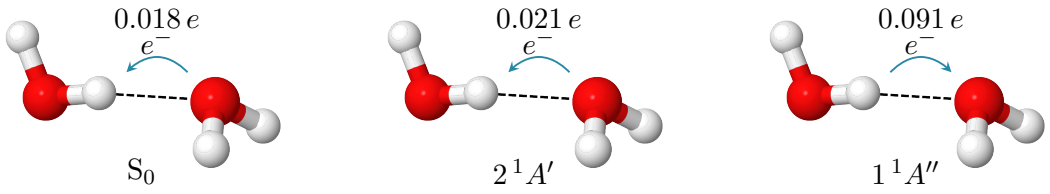

Figure 3: Intermolecular charge transfer diagram in $(H_2O)_2$ at the S_0 equilibrium geometry for its ground and its two first singlet electronic excited states in the $\mathcal{C}_s$ point group.

Table 2: Atomic charges within the water dimer in both the ground state and the first singlet excited states of $(H_2O)_2$[†] The last column is the delocalisation index (DI) between the two H_2O units of the dimer, and the values in the row below each excited state indicate changes with respect to the ground state.

	Atomic charges					
	H-bond donor			H-bond acceptor		
State	q^{O2}	q^{H3}	q^{H4}	q^{O1}	q^{H5}	DI
GS	−1.215	0.627	0.570	−1.170	0.594	0.137
$2\,^1A'$	−1.166	0.560	0.585	−0.861	0.441	0.194
	0.049	−0.067	0.015	0.309	−0.153	0.057
$1\,^1A''$	−0.903	0.704	0.290	−1.266	0.588	0.344
	0.312	0.077	−0.280	−0.096	−0.006	0.207

[†] The q^O (q^H) atomic charges in the S_0 and S_1 states of the H_2O molecule are −1.166 (0.583) and −0.884 (0.441), respectively in accordance with Table 1.

merely mention that these explanations rely on the molecular polarization induced on each monomer by the electric field created by its interacting partner.

This similarity is broken in the EES, where considerable differences between the HB acceptor and HB donor appear, on top of those brought about by the hydrogen bond (Table 2). The QTAIM charges uncover that it is only one of the two molecules that gets excited upon photoabsorption of the dimer, and that this molecule is different in the $1\,^1A''$ and $2\,^1A'$ EES. The atomic charges of the HB acceptor in the $2\,^1A'$ state resemble those of the S_1 H_2O molecule while the HB donor mirror those of the GS as revealed by the first two lines of Table 2 and the upper part of Table 1. The situation is reversed in the $1\,^1A''$ EES. This closeness of QTAIM charges is evidenced by the fact that the oxygen atom of an isolated water molecule losses about 0.28 electrons as a result of the $S_0 \rightarrow S_1$ excitation (third row of Table 1) while those of the HB acceptor in the $2\,^1A'$ EES and the HB donor in the $1\,^1A''$ state are each deprived of 0.31 electrons (last and antepenultimate row of Table 2) with respect to the corresponding atoms in GS. The blue shift in the $2\,^1A'$ EES is related to a photon being absorbed by the HB acceptor whereas the red shift in the $1\,^1A''$ EES corresponds to a photoexcitation of the H-bond donor.

We get further relevant information after considering the IQA partition. Each of the

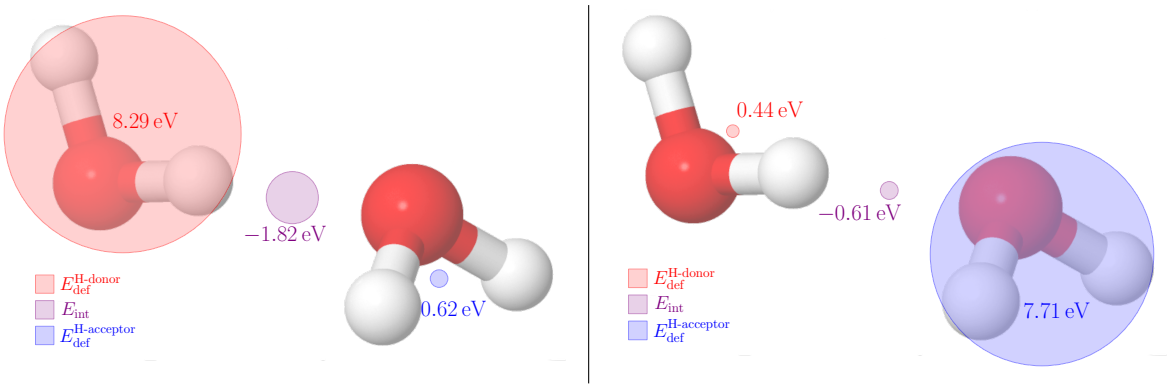

Figure 4: Deformation energy (with respect to the isolated monomer in the ground state) of the two water molecules in the the $1\,^1A''$ (left) and $2\,^1A'$ EES (right) of $(H_2O)_2$ at the S_0 equilibrium geometry. The total interfragment interaction energy is also shown for completeness. The $S_0 \rightarrow S_1$ excitation energy in water is 7.41 eV. The data are reported in eV.

molecules suffers a change in its net energy (i.e. they are subject to a deformation energy) as well as an alteration in their interaction on photoexcitation. We consider first the deformation energy of each fragment, $E_{\text{def}}^{A} = E_{\text{net}}^{A} - E_{\text{net},0}^{A}$, viz., the change in the net energy with respect to that in the isolated H_2O molecule in its GS. The values of $E_{\text{def}}^{H_2O}$ of the HB donor and HB acceptor in the GS of $(H_2O)_2$ are 0.41 eV and 0.28 eV respectively. As shown in Figure 4, the deformation energy of the HB donor in the $2\,^1A'$ EES and the HB acceptor in the $1\,^1A''$ EES are close to those found in the GS dimer. The values of $E_{\text{def}}^{H_2O}$ for the interacting partner in both states is much higher and they resemble the value of the $S_0 \rightarrow S_1$ excitation energy of the water monomer, i.e., 7.41 eV. We then have a slightly distorted and a photoexcited monomer in the $1\,^1A''$ and $1\,^1A''$ EES of $(H_2O)_2$. Tables S19–S21 in the ESI show that $E_{\text{def}}^{H_2O}$ for the GS monomer and $E_{\text{int}}^{H_2O\cdots H_2O}$ converge to zero as the intermolecular distance is increased. Ditto for $E_{\text{def}}^{H_2O}$ of the photoexcited fragment, which approaches the $S_0 \rightarrow S_1$ excitation energy of the monomer when $R_{O\cdots O}$ tends to infinity.

The dissection of the intermolecular IQA interaction energy for the ground state, $1\,^1A''$ and $2\,^1A'$ EES of $(H_2O)_2$ is displayed in Figure 5, which contains the basic rationale for the understanding of the double hypso- and bathochromic shifts in $(H_2O)_2$. $E_{\text{int}}^{H_2O\cdots H_2O}$ takes a value of −0.96 eV in the GS, which corresponds roughly to 25 % ionic (−0.24 eV) and 75 % covalent (−0.72 eV). The total deformation of the two fragments (0.68 eV) compensates much

of the covalent term, an observation which allows an electrostatic interpretation of hydrogen bonding. The $1\,^1A''$ state was previously identified with an HB donor excitation. This EES presents an enhanced intermolecular interaction energy of $-1.80\,\mathrm{eV}$, which is almost twice that computed for the GS. As indicated in the bottom-left part of Figure 5, this increase in the magnitude of the IQA interaction energy comes from both the exchange-correlation ($-1.17\,\mathrm{eV}$) along with the classical ($-0.64\,\mathrm{eV}$) components and it can be rationalised as follows. The atoms with the most negative and most positive charge in Table 2 are respectively the oxygen of the HB acceptor and the H atom involved in the HB of the $1\,^1A''$ EES. These atoms have the closest intermolecular contacts and hence the increase of the magnitude of their charges with opposite signs will result in a more stabilising value of $E_{\mathrm{class}}^{\mathrm{H_2O\cdots H_2O}}$. On the other hand, the rise of $|E_{\mathrm{xc}}^{\mathrm{H_2O\cdots H_2O}}|$ in the $1\,^1A''$ EES with respect to GS is consistent with the increase of the intermolecular DI between monomers as a result of photoabsorption as indicated in the last column of Table 2.

Contrariwise, the intermolecular interaction energy in the $2\,^1A'$ EES decreases with respect to that in the GS dimer, and now the corresponding changes in covalent ($E_{\mathrm{xc}}^{\mathrm{H_2O\cdots H_2O}}$) and ionic ($E_{\mathrm{class}}^{\mathrm{H_2O\cdots H_2O}}$) contributions have opposite signs (top-right part of Figure 5). The exchange-correlation term ($-0.8\,\mathrm{eV}$) exhibits a slight increase in magnitude in regard to the corresponding value in the S_0 state The exchange-correlation term ($-0.8\,\mathrm{eV}$) exhibits a slight increase in magnitude in regard to the corresponding value in the S_0 state ($-0.72\,\mathrm{eV}$). But more importantly, the classical component changes from attractive ($-0.24\,\mathrm{eV}$) to repulsive ($0.19\,\mathrm{eV}$) as a result of photoexcitation. Once again, this change of the classical component of the interaction energy can be understood on the basis of the atomic charges reported in Table 2. The oxygen of the HB acceptor and the H atom entailed in the H-bond in the $2\,^1A'$ EES become respectively less negative and less positive with respect to the same atoms in the GS. This condition contributes to the desestabilising nature of $E_{\mathrm{class}}^{\mathrm{H_2O\cdots H_2O}}$ in this EES. As a matter of fact, the oxygen of the HB acceptor in the $2\,^1A'$ EES is considerably the less negative O atom in Table 2. This situation is opposite to that occurring in the $1\,^1A''$ EES discussed above.

Figure 6 shows the differences in the intermolecular interaction energy components for

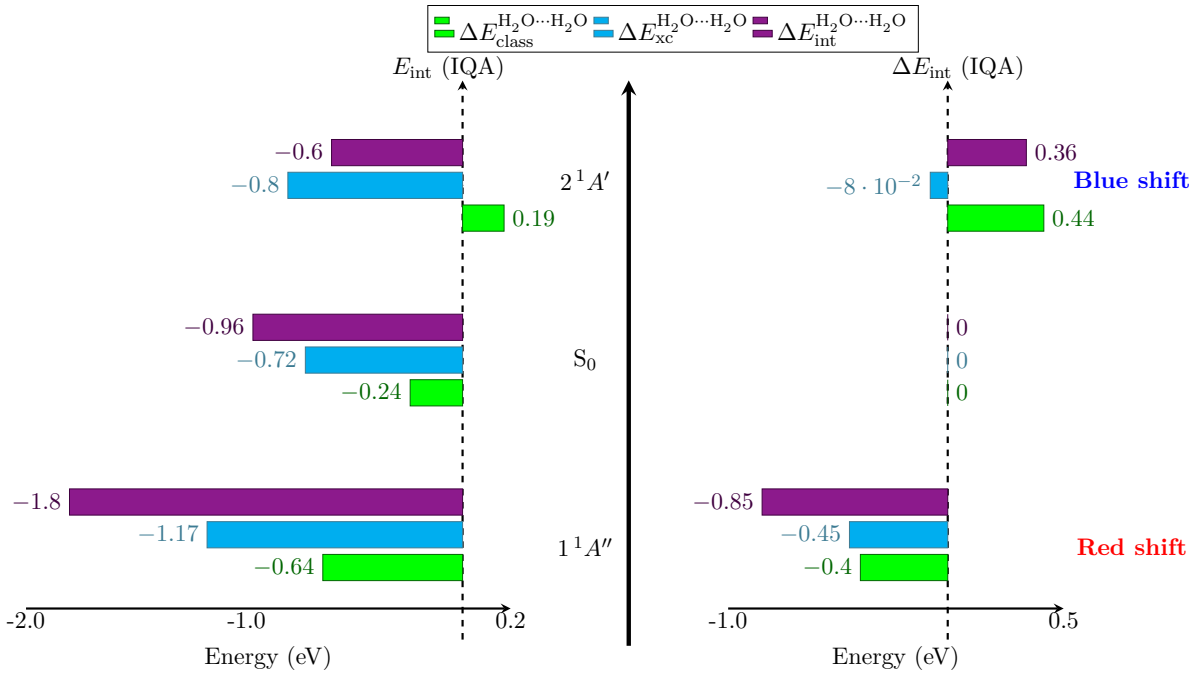

Figure 5: (Left) Components in the intermolecular IQA interaction energies in the $2\,^1A'$, S_0 and the $1\,^1A''$ states of $(H_2O)_2$ at the ground state equilibrium geometry. The states are arranged in a descending order of $E_{\text{int}}^{H_2O\cdots H_2O}$ (indicated in purple) from top to bottom. (Right) Change in these contributions for the the $2\,^1A'$ and the $1\,^1A''$ excited states with respect to the ground state. The data are reported in eV.

the $2\,^1A'$ and $1\,^1A''$ EES of $(H_2O)_2$ with respect to those of the S_0 state as a function of the O···O distance. As expected, there is barely any difference between the two states at large O···O distances. When the two H_2O units approach each other, the values of ΔE_{int} for both EES follow a pattern very similar to that of excitation energy shown in Figure 2, i.e., $\Delta E_{\text{int}}^{2\,^1A'}$ increases while $\Delta E_{\text{int}}^{1\,^1A''}$ exhibits the opposite behaviour. Regarding the exchange-correlation term of the interaction energy, we observe that $\Delta E_{\text{xc}}^{1\,^1A''}$ is more negative than $\Delta E_{\text{xc}}^{2\,^1A'}$ in the whole range of O···O distances. On the other hand, the classical terms behave very differently: $\Delta E_{\text{class}}^{2\,^1A'}$ is always positive while $\Delta E_{\text{class}}^{1\,^1A''}$ starts being small and positive at large O···O distances, reaches a maximum at around 5 Å and then becomes large and negative for shorter O···O distances. We can better understand this behaviour via a simple classical model for the interaction between the water monomers in the investigated electronic states of $(H_2O)_2$ based on their in-the-cluster dipole moments as described below.

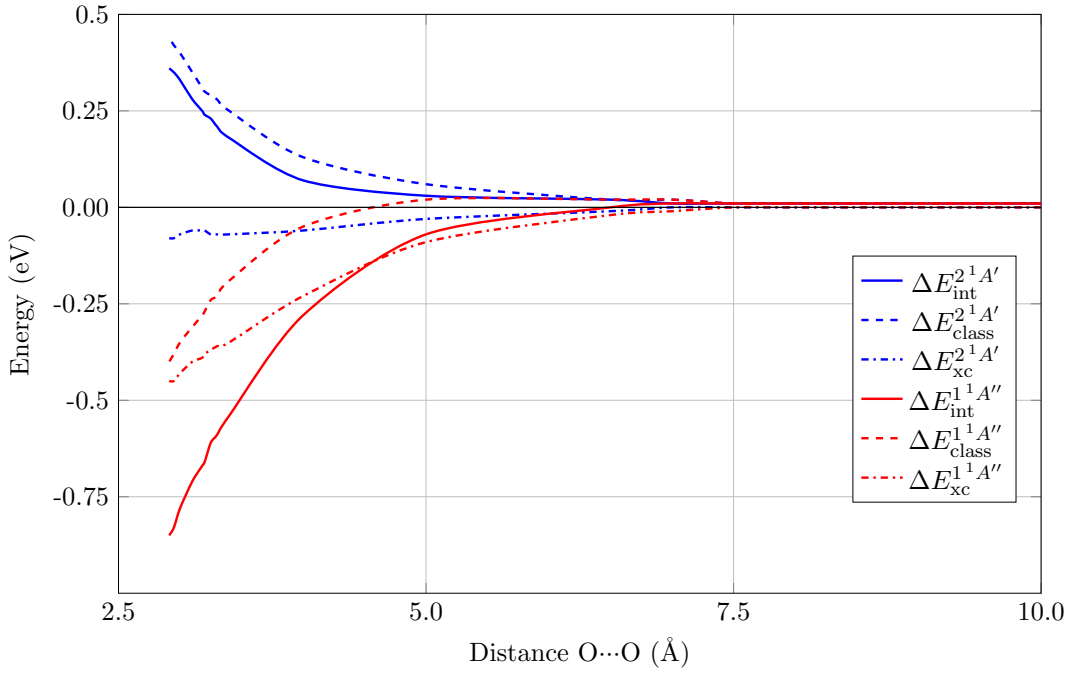

Figure 6: Differences in the IQA intermolecular interaction energies of the $2\,^1A'$ and $1\,^1A''$ excited states of $(H_2O)_2$ with respect to the corresponding values in the ground state.

Hypsochromic and bathochromic responses of $(H_2O)_2$ as a result of two interacting molecular dipoles

Thanks to the above-mentioned real space analysis, we can rigorously use all the traditional tools available in the theory of intermolecular interactions to follow the evolution of the excitation energies at any intermolecular distance regime. The chemical community has developed much of their intuitive understanding of intermolecular interactions in the long-range regime, wherein symmetry adapted perturbation theory (SAPT),[69] or even the polarization approximation can be used. Intermolecular interaction energies are considered as the result of first order electrostatic and exchange-repulsion effects, and second order induction and dispersion contributions. The electrostatic component can be further partitioned via multipolar expansions. Of course, this successful perturbation framework is built from unperturbed, isolated molecular descriptors (e.g. molecular multipole moments and polarizabilities) and it breaks apart at short range, where perturbation theory cannot be applied anymore and the unperturbed molecular picture is not applicable. The properties of interacting molecules can

notwithstanding be recovered at long and short ranges on the basis of QCT. We now show that much of the traditional insights about multipole-multipole interactions are still operative at short-range when we use the perturbed, in-the-cluster multipoles instead of those of the isolated species.

Let us then consider a minimal working model of the water dimer which corresponds to that of two interacting dipoles. For this purpose we recall the explicit expression[70] for the interaction energy between two dipoles, $U_{\boldsymbol{\mu}^A\boldsymbol{\mu}^B}$,

$$U_{\boldsymbol{\mu}^A\boldsymbol{\mu}^B} = \frac{R^2\boldsymbol{\mu}^A\cdot\boldsymbol{\mu}^B - 3(\boldsymbol{\mu}^A\cdot\boldsymbol{R})(\boldsymbol{\mu}^B\cdot\boldsymbol{R})}{4\pi\epsilon_0 R^5}, \tag{12}$$

where $\boldsymbol{\mu}^A$ and $\boldsymbol{\mu}^B$ represent the dipole moments of units A and B, respectively, and $\boldsymbol{R}$ is the intermolecular distance vector. The molecular multipoles of each fragment *can be defined unambiguously* in the QTAIM once appropriate reference frame origins are chosen for each of them. We have use the naïve center of mass of each molecule. Since the fragments are slightly non-neutral, we warn that all non-monopole multipolar interaction terms are origin dependent, although their sum is not (in the case of convergence). We can obtain in this way the dipole-dipole contribution of the two interacting molecules.

Figure 7 shows that $U_{\boldsymbol{\mu}^A\boldsymbol{\mu}^B}$ is attractive at all O···O distances in the ground state. Since the excitations which conduce to the $2\,^1A'$ and $1\,^1A''$ EES of $(H_2O)_2$ is accompanied by the inversion of the dipole of the HB acceptor or donor respectively, we observe a hypsochromic effect for both EES at large O···O distances (right part of Figure 7). As the two H_2O units approach each other, the repulsion slightly increases for both excited states (region between long-range and mid-range in Figure 7). The interaction gets more complex for O···O distances in the short-range regime: the dipole-dipole interaction for the $2\,^1A'$ state becomes more repulsive while that corresponding to the $1\,^1A''$ state turn into attractive.

Most interestingly, the dipole-dipole interaction follows closely the changes in the total electrostatic (classical) interaction shown in Figure 6. Moreover, the evolution of the dipole-dipole term is sufficient to explain qualitatively the hypsochromic and bathochromic effects of Figure 2. Despite the relevance of the exchange-correlation (covalent) contribution, the interaction in the examined electronic states of the water dimer can be understood in terms

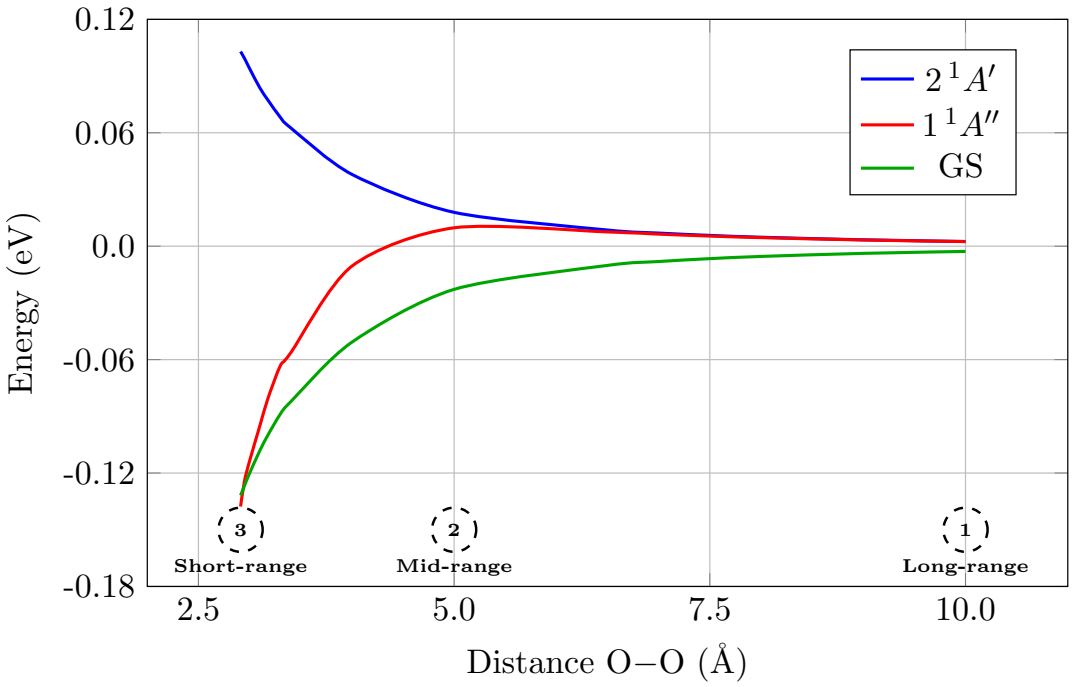

Figure 7: Intermolecular dipole-dipole interactions for the ground state and the $1\,^1A''$ and $2\,^1A'$ EES of the H_2O dimer.

of dipole-dipole electrostatics, in a very similar fashion to the Buckingham-Fowler model.[71]

As expected, the molecular in-the-cluster dipoles of the interacting water molecules in the $1\,^1A''$, $2\,^1A'$ and S_0 states of $(H_2O)_2$ change with the intermolecular distance. Figure 8 schematise the dipoles and the attractive or repulsive character of their interaction, at three selected O···O distances in the short-, mid-, and long-range regimes. The ground state (bottom of Figure 8) presents an attractive head-to-tail configuration in consistency with the corresponding potential energy curve of Figure 7. The dipolar electric fields of the HB donor and HB acceptor in the S_0 state of $(H_2O)_2$ reinforce the molecular dipoles upon interaction, in agreement with our standard knowledge of molecular polarization in hydrogen bonds. The magnitude of the interacting dipoles significantly increases as the intermolecular distance decreases: $|\boldsymbol{\mu}|$ rises 11 and 5 % for the HB donor and HB acceptor respectively, when going from the isolated monomers to the equilibrium geometry in the S_0 state of $(H_2O)_2$ (see Tables S22–S25 in the ESI). The situation changes completely when photoexcitation occurs. We start by considering the dipole inversion in the long-range regime of the HB donor and the

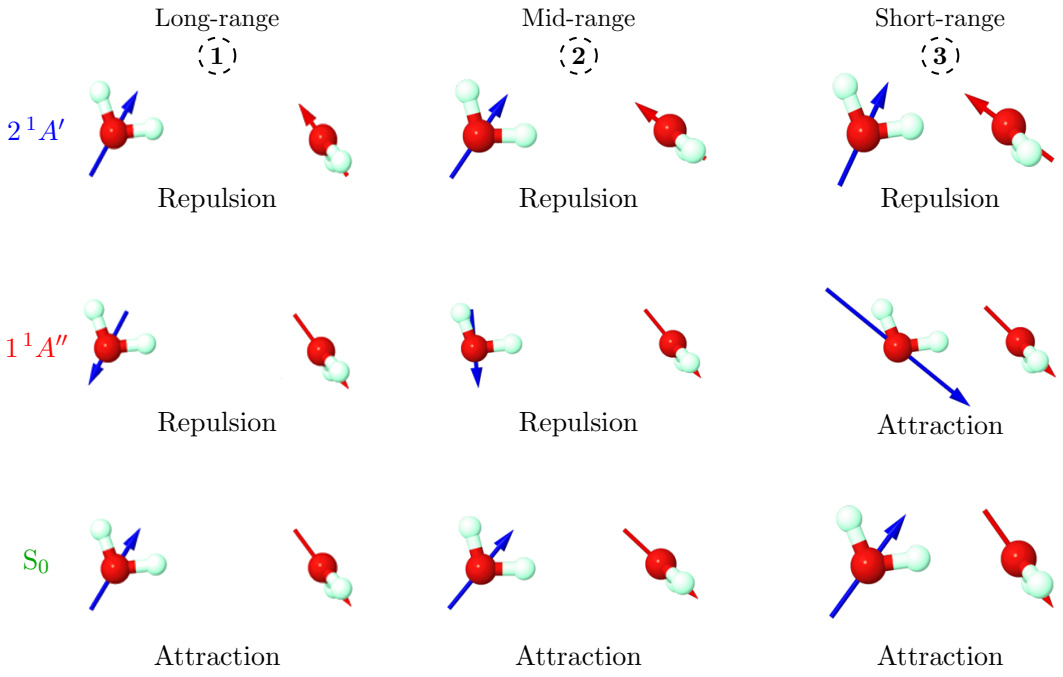

Figure 8: Relative magnitude and orientation of the in-the-cluster dipoles in the ground, $2\,^1A'$ and $1\,^1A''$ states of the water dimer at the O···O distances of 10 Å (left), 5 Å (center), and 2.0 Å (right).

HB acceptor in the $1\,^1A''$, $2\,^1A'$ EES respectively as shown in the left part of Figure 8. This observation reinforces the idea that it is the HB donor that gets excited in the $1\,^1A''$ EES of $(H_2O)_2$. Ditto for the HB acceptor in the $2\,^1A'$ EES of the water dimer. The resulting head-to-head (in the $2\,^1A'$ EES) and tail-to-tail (in the $1\,^1A''$ EES) are clearly repulsive. In other words, photoexcitation leading to the $1\,^1A''$ and $2\,^1A'$ EES of $(H_2O)_2$ results in a destabilising electrostatic interaction at long intermolecular distances. When the molecules get closer, polarization leads to a dipole moment enhancement, as it occurs in the S_0 state. Regarding the $1\,^1A''$ EES the dipole of the HB donor not only increases, but it also undergoes a crucial rotation that leads to a clearly attractive dipole-dipole configuration as the O···O distance decreases. The character of the interaction changes from destabilising to stabilising at about $R_{O\cdots O} = 4.4$ Å. We underscore that the two water molecules respond very differently in the $1\,^1A''$ EES of $(H_2O)_2$ when the two fragments approach each other. Only the dipole of the HB donor, i.e. the photoexcited monomer in the $1\,^1A''$ state, suffers a dramatic change. Its magnitude is increased by 120 % at the S_0 equilibrium geometry as opposed to that of

the HB acceptor which is raised by only 5 %. This general phenomenon of dipole moment enhancement is observed not only in the S_0 and $1\,^1A''$ states of the water dimer but also in condensed phases, and it is of paramount importance in the tailoring of non-linear optical properties in molecular crystals.[72]

The dipole moments of the monomers in the $2\,^1A'$ EES change much less with $R_{O\cdots O}$ as compared to those in the $1\,^1A''$ EES. There is essentially no rotation of any of these vectors and their magnitude change respectively by -0.1 and 8.0 % for the HB donor and HB acceptor from the long range regime to the S_0 equilibrium geometry. We hypothesise that the excitation of the HB acceptor in the $2\,^1A'$ EES of $(H_2O)_2$ heavily modifies the lone pairs of the acceptor oxygen, impairing the formation of the HB at any distance. This situation is to be contrasted with that of the $1\,^1A''$ EES wherein the HB accepting lone pair is not severely affected by photoexcitation, and the electron structure of the donor molecule readapts until a favorable interaction takes place. This possibility should be explored in larger clusters.

To summarise, photoexcitation drastically alters the interaction between the two H_2O units in the dimer as compared to that in the ground state. In the latter, the dipole-dipole configuration is attractive with a relatively constant orientation throughout the whole potential energy curve. The inversion of the dipole moment in the HB acceptor molecule in the $2\,^1A'$ EES of $(H_2O)_2$ results in a sustained repulsive interaction, that explains the observed hypsochromic effect. On the other hand, the dipole moment of the photoexcited HB donor in the $1\,^1A''$ EES of the water dimer suffers a rotation that renders a stabilising interaction at short range and thereby a bathochromic excitation energy shift.

Perspectives for future studies in photochemistry

We consider now briefly how the techniques employed in this investigation can be further exploited in photochemistry. The IQA analysis requires the one- and two-electron matrices to partition the electronic energy of any given electronic state (either ground or excited). Hence, the IQA energy partition can in principle be coupled with any electronic structure method which provides wavefunctions of electronic excited states. The computation of 1-RDM and 2-RDM can be somewhat more complicated for non-variational approximations because of

the calculation of Lagrangian density functions as it is the case of coupled cluster[73] or perturbation theory methods.[74–76] It would also be desirable to couple the IQA energy partition with TDDFT for the study of excited states as it is done in ground state with DFT.[77,78] Regarding studies in condensed phase, we could also consider snapshots of molecular dynamics simulations to see how the different orientations of the interacting monomers affect the energy distribution of the system. One can also address, of course, other H-bonded excited dimers such as the the ammonia dimer,[79] formaldehyde dimer,[80] formic acid dimer[81,82] along with its thioderivative[83] or heterodimers[84] of amines and carboxylic acids relevant in excited state double proton transfers.[35] A final perspective for the exploitation of the methos considered herein is the investigation of the effect of solvent or protein cavities in the partition of the excitation energy of chromophores. For this endeavour, one would have to consider how either the solvent or peptidic sorroundings modify the one and two-electron matrices of the examined excited state. Some progress in this direction have been made for the effects of the solvent in the IQA energy partition in ground state.[85]

Concluding remarks

We have convincingly shown in this contribution how real space QCT techniques can be used to exploit chemically intuitive ideas in photochemistry. To that end, we have explored the chemical origin of solvatochromic effects via the examination of the hypsochromic and bathochromic shifts caused by hydrogen bonding in $(H_2O)_2$. QCT allows to maintain the perturbative language of the theory of intermolecular interactions even for strongly interacting systems, both in ground and excited states. The methods used in this investigation also permit us to compute and explore in-the-cluster molecular properties in a rigorous way, and thereby to apply chemically intuitive concepts to any system in a wide variety of electronic states using a broad battery of low to high quality electronic structure methods. We have shown that the two examined EES of $(H_2O)_2$ are associated with localised excitations in either the H-bond donor or acceptor. These excited moieties interact with the ground state partner in the molecular cluster. Besides non-negligible covalent contributions which are well-understood in hydrogen bonds in the ground state, the basic conditions that lead to the double red and blue

shifts of $(H_2O)_2$ addressed herein can be rationalised through in-the-cluster molecular dipoles. The excitation of one of the monomers leads to an inversion of its dipole moment. This change in electronic structure conduces to an hypsochromic shift at long range for the two $2\,^1A'$ and $1\,^1A''$ EES of $(H_2O)_2$. Nonetheless, the evolution of the in-the-cluster dipoles differs in these two EES throughout the corresponding potential energy curves. Such evolution explains in a very appealing way the double hypso- and bathochromic shifts of $(H_2O)_2$. We firmly think that the use of the methods and ideas exploited in this investigation may be of wide interest to rationalise and gain valuable insights about photochemical problems.

Acknowledgements

We gratefully acknowledge financial support from CONACyT/Mexico (grant 253776 and PhD scholarship 436154 for AFA), PAPIIT/UNAM (project IN205118), the Spanish MICINN (grant PGC2018-095953-B-I00), and the Principado de Asturias Government (grant FC-GRUPIN-IDI/2018/000117). We are also grateful to DGTIC/UNAM (grant LANCAD-UNAM-DGTIC-250) for computer time.

References

[1] P. Coppens, *Angew. Chem. Int. Ed.* **2009**, *48*, 4280–4281.

[2] Z. Ji, G. Natu, Z. Huang, O. Kokhan, X. Zhang, Y. Wu, *J. Phys. Chem. C* **2012**, *116*, 16854–16863.

[3] T. C. Sum, N. Mathews, *Energy Environ. Sci.* **2014**, *7*, 2518–2534.

[4] K. Sato, K. Shizu, K. Yoshimura, A. Kawada, H. Miyazaki, C. Adachi, *Phys. Rev. Lett.* **2013**, *110*.

[5] W. P. Gillin, S. Zhang, N. J. Rolfe, P. Desai, P. Shakya, A. J. Drew, T. Kreouzis, *Phys. Rev. B* **2010**, *82*, 195208.

[6] A. Fermi, G. Bergamini, M. Roy, M. Gingras, P. Ceroni, *J. Amer. Chem. Soc.* **2014**, *136*, 6395–6400.

[7] T. L. Mako, J. M. Racicot, M. Levine, *Chem. Rev.* **2018**, *119*, 322–477.

[8] M. Shimizu, T. Hiyama, *Chem.: Asian. J.* **2010**, *5*, 1516–1531.

[9] J. Rajput, D. B. Rahbek, L. H. Andersen, T. Rocha-Rinza, O. Christiansen, K. B. Bravaya, A. V. Erokhin, A. V. Bochenkova, K. M. Solntsev, J. Dong, J. Kowalik, L. M. Tolbert, M. Å. Petersen, M. B. Nielsen, *Phys. Chem. Chem. Phys.* **2009**, *11*, 9996.

[10] T. Rocha-Rinza, O. Christiansen, J. Rajput, A. Gopalan, D. B. Rahbek, L. H. Andersen, A. V. Bochenkova, A. A. Granovsky, K. B. Bravaya, A. V. Nemukhin, K. L. Christiansen, M. B. Nielsen, *J. Phys. Chem. A* **2009**, *113*, 9442–9449.

[11] H. Chosrowjan, N. Mataga, Y. Shibata, Y. Imamoto, F. Tokunaga, *J. Phys. Chem. B* **1998**, *102*, 7695–7698.

[12] M. Vengris, I. H. M. van Stokkum, X. He, A. F. Bell, P. J. Tonge, R. van Grondelle, D. S. Larsen, *J. Phys. Chem. A* **2004**, *108*, 4587–4598.

[13] K. Bravaya, A. Bochenkova, A. Granovsky, A. Nemukhin, *J. Amer. Chem. Soc.* **2007**, *129*, 13035–13042.

[14] V. R. I. Kaila, R. Send, D. Sundholm, *J. Phys. Chem. B* **2012**, *116*, 2249–2258.

[15] O. Valsson, P. Campomanes, I. Tavernelli, U. Rothlisberger, C. Filippi, *J. Chem. Theory Comput.* **2013**, *9*, 2441–2454.

[16] S. L. Logunov, L. Song, M. A. El-Sayed, *J. Chem. Phys.* **1996**, *100*, 18586–18591.

[17] M. Irie, T. Fukaminato, T. Sasaki, N. Tamai, T. Kawai, *Nature* **2002**, *420*, 759–760.

[18] W. Szymański, J. M. Beierle, H. A. V. Kistemaker, W. A. Velema, B. L. Feringa, *Chem. Rev.* **2013**, *113*, 6114–6178.

[19] J. Calbo, C. E. Weston, A. J. P. White, H. S. Rzepa, J. Contreras-García, M. J. Fuchter, *J. Amer. Chem. Soc.* **2017**, *139*, 1261–1274.

[20] Q. Zhao, C. Huang, F. Li, *Chem. Soc. Rev.* **2011**, *40*, 2508.

[21] Y. Yang, Q. Zhao, W. Feng, F. Li, *Chem. Rev.* **2012**, *113*, 192–270.

[22] J. Chan, S. C. Dodani, C. J. Chang, *Nat. Chem.* **2012**, *4*, 973–984.

[23] S. Shirai, S. Iwata, T. Tani, S. Inagaki, *J. Phys. Chem. A* **2011**, *115*, 7687–7699.

[24] C. E. Crespo-Hernández, B. Cohen, B. Kohler, *Nature* **2005**, *436*, 1141–1144.

[25] B. Mondal, T. Zhang, R. Prabhakar, B. Captain, V. Ramamurthy, *Photochem. Photobiol. Sci.* **2014**, *13*, 1509–1520.

[26] A. Toniolo, S. Olsen, L. Manohar, T. J. Martínez, *Faraday Discuss.* **2004**, *127*, 149–163.

[27] J. Dong, K. M. Solntsev, L. M. Tolbert, *J. Amer. Chem. Soc.* **2006**, *128*, 12038–12039.

[28] T. Rocha-Rinza, K. Sneskov, O. Christiansen, U. Ryde, J. Kongsted, *Phys. Chem. Chem. Phys.* **2011**, *13*, 1585–1589.

[29] G.-J. Zhao, K.-L. Han, *J. Phys. Chem. A* **2007**, *111*, 9218–9223.

[30] G.-J. Zhao, K.-L. Han, *J. Phys. Chem. A* **2009**, *113*, 14329–14335.

[31] A. Magnuson, H. Berglund, P. Korall, L. Hammarström, B. Åkermark, S. Styring, L. Sun, *J. Amer. Chem. Soc.* **1997**, *119*, 10720–10725.

[32] L. Sun, M. Burkitt, M. Tamm, M. K. Raymond, M. Abrahamsson, D. LeGourriérec, Y. Frapart, A. Magnuson, P. H. Kenéz, P. Brandt, A. Tran, L. Hammarström, S. Styring, B. Åkermark, *J. Amer. Chem. Soc.* **1999**, *121*, 6834–6842.

[33] D. M. Manuta, A. J. Lees, *Inorg. Chem.* **1986**, *25*, 3212–3218.

[34] N. S. Hush, J. R. Reimers, *Chem. Rev.* **2000**, *100*, 775–786.

[35] P. Zhou, K. Han, *Acc. Chem. Res.* **2018**, *51*, 1681–1690.

[36] D. González, O. Neilands, M. C. Rezende, *J. Chem. Soc. Per. Trans. 2* **1999**, 713–718.

[37] J. Segarra-Martí, D. Roca-Sanjuán, M. Merchán, R. Lindh, *J. Chem. Phys.* **2012**, *137*, 244309.

[38] Z. S. Huang, R. E. Miller, *J. Chem. Phys.* **1989**, *91*, 6613–6631.

[39] J. N. Harvey, J. O. Jung, R. B. Gerber, *J. Chem. Phys.* **1998**, *109*, 8747–8750.

[40] D. Jacquemin, L. Blancafort, Y. M. Rhee, *ChemPhotoChem* **2019**, *3*, 664–665.

[41] J. M. Herbert, M. Head-Gordon, *J. Amer. Chem. Soc.* **2006**, *128*, 13932–13939.

[42] C. Morell, V. Labet, A. Grand, P. W. Ayers, F. D. Proft, P. Geerlings, H. Chermette, *J. Chem. Theory Comput.* **2009**, *5*, 2274–2283.

[43] L. Vannay, E. Brémond, P. de Silva, C. Corminboeuf, *Chem.: Eur. J.* **2016**, *22*, 18442–18449.

[44] Q. Ge, Y. Mao, M. Head-Gordon, *J. Chem. Phys.* **2018**, *148*, 064105.

[45] Q. Ge, M. Head-Gordon, *J. Chem. Theory Comput.* **2018**, *14*, 5156–5168.

[46] N. V. Tkachenko, A. I. Boldyrev, *Phys. Chem. Chem. Phys.* **2019**, *21*, 9590–9596.

[47] R. McWeeny, *Methods of Molecular Quantum Mechanics 2nd ed.*, Academic Press, London, **1992**, Chapter 14.

[48] R. F. W. Bader, *Atoms in Molecules. A Quantum Theory*, Oxford University Press, Oxford, **1995**.

[49] A. D. Becke, K. E. Edgecombe, *J. Chem. Phys.* **1990**, *92*, 5397.

[50] M. A. Blanco, A. Martín Pendás, E. Francisco, *J. Chem. Theory Comput.* **2005**, *1*, 1096–1109.

[51] E. Francisco, A. M. Pendás, M. A. Blanco, *J. Chem. Theory Comput.* **2005**, *2*, 90–102.

[52] R. Ponec, *J. Math. Chem.* **1997**, *21*, 323–333.

[53] R. Ponec, *J. Math. Chem.* **1998**, *23*, 85–103.

[54] M. Menéndez, R. Ávarez Boto, E. Francisco, A. Martín Pendás, *J. Comput. Chem.* **2015**, *36*, 833–843.

[55] P. B. Coto, D. Roca-Sanjuán, L. Serrano-Andrés, Á. Martín-Pendás, S. Martí, J. Andrés, *J. Chem. Theory Comput.* **2009**, *5*, 3032–3038.

[56] D. Ferro-Costas, Á. M. Pendás, L. González, R. A. Mosquera, *Phys. Chem. Chem. Phys.* **2014**, *16*, 9249–9258.

[57] L. A. Terrabuio, R. L. A. Haiduke, C. F. Matta, *Theor. Chem. Acc.* **2016**, *135*.

[58] L. A. Terrabuio, N. A. da Silva, R. L. A. Haiduke, C. F. Matta, *Mol. Phys.* **2017**, *115*, 1955–1965.

[59] J. Jara-Cortés, J. M. Guevara-Vela, Á. Martín Pendás, J. Hernández-Trujillo, *J. Comput. Chem.* **2017**, *38*, 957–970.

[60] S. Mitra, A. K. Chandra, P. M. Gashnga, S. Jenkins, S. R. Kirk, *J. Mol. Model.* **2012**, *18*, 4225–4237.

[61] M. X. Hu, T. Xu, R. Momen, G. Huan, S. R. Kirk, S. Jenkins, M. Filatov, *J. Comput. Chem.* **2016**, *37*, 2588–2596.

[62] J. Jara-Cortés, T. Rocha-Rinza, J. Hernández-Trujillo, *Comput. Theor. Chem.* **2015**, *1053*, 220–228.

[63] A. Fernández-Alarcón, J. L. Casals-Sainz, J. M. Guevara-Vela, A. Costales, E. Francisco, Á. M. Pendás, T. Rocha-Rinza, *Phys. Chem. Chem. Phys.* **2019**, *21*, 13428–13439.

[64] Á. Martín Pendás, E. Francisco, *ChemPhysChem* **2019**, *20*, 2722–2741.

[65] C. Outeiral, M. A. Vincent, Á. Martín Pendás, P. L. A. Popelier, *Chem. Sci.* **2018**, *9*, 5517–5529.

[66] E. Francisco, D. Menéndez Crespo, A. Costales, A. Martín Pendás, *J. Comput. Chem.* **2017**, 1–14.

[67] J. L. Casals-Sainz, J. Jara-Cortés, J. Hernández-Trujillo, J. M. Guevara-Vela, E. Francisco, Á. Martín Pendás, *Chem.: Eur. J.* **2019**, *25*, 12169–12179.

[68] A. Martín Pendás, M. A. Blanco, E. Francisco, *J. Chem. Phys.* **2006**, *125*, 184112.

[69] B. Jeziorski, R. Moszynski, K. Szalewicz, *Chem. Rev.* **1994**, *94*, 1887.

[70] A. Stone, *The Theory of Intermolecular Forces*, Oxford University Press, **2016**.

[71] D. A. Buckingham, P. W. Fowler, *J. Chem. Phys.* **1983**, *79*, 6426.

[72] M. A. Spackman, P. Munshi, B. Dittrich, *ChemPhysChem* **2007**, *8*, 2051–2063.

[73] F. J. Holguín-Gallego, R. Chávez-Calvillo, M. García-Revilla, E. Francisco, Á. M. Pendás, T. Rocha-Rinza, *J. Comput. Chem.* **2016**, *37*, 1753–1765.

[74] J. L. McDonagh, A. F. Silva, M. A. Vincent, P. L. A. Popelier, *J. Phys. Chem. Lett.* **2017**, *8*, 1937–1942.

[75] A. F. Silva, P. L. A. Popelier, *J. Mol. Model.* **2018**, *24*, 201.

[76] V. Tognetti, A. F. Silva, M. A. Vincent, L. Joubert, P. L. A. Popelier, *J. Phys. Chem. A* **2018**, *122*, 7748–7756.

[77] P. Maxwell, Á. M. Pendás, P. L. A. Popelier, *Phys. Chem. Chem. Phys.* **2016**, *18*, 20986–21000.

[78] E. Francisco, J. L. Casals-Sainz, T. Rocha-Rinza, A. M. Pendás, *Theor. Chem. Acc.* **2016**, *135*.

[79] P. Farmanara, H.-H. Ritze, V. Stert, W. Radloff, I. V. Hertel, *J. Chem. Phys.* **2002**, *116*, 1443–1456.

[80] A. A. Voityuk, *J. Phys. Chem. B* **2014**, *119*, 7417–7421.

[81] J. Novak, M. Mališ, A. Prlj, I. Ljubić, O. Kühn, N. Došlić, *J. Phys. Chem. A* **2012**, *116*, 11467–11475.

[82] S. Giri, R. Parida, M. Jana, S. Gutiérrez-Oliva, A. Toro-Labbe, *J. Phys. Chem. A* **2017**, *121*, 9531–9543.

[83] Á. Cimas, O. Mó, M. Yáñez, N. Martín, I. Corral, *Phys. Chem. Chem. Phys.* **2010**, *12*, 13037.

[84] F.-T. Hung, W.-P. Hu, T.-H. Li, C.-C. Cheng, P.-T. Chou, *J. Phys. Chem. A* **2003**, *107*, 3244–3253.

[85] F. Jiménez-Grávalos, N. Díaz, E. Francisco, Á. Martín-Pendás, D. Suárez, *ChemPhysChem* **2018**, *19*, 3425–3435.